Chapter 28

Suspended Sand and Bedload Transport on Beaches

Nobuhisa Kobayashi
Center for Applied Coastal Research
University of Delaware, Newark, DE 19716, USA
nk@coastal.udel.edu

Andres Payo
Graduate School of Science and Technology
University of Kumamoto, 2-39-1, Kurokami
Kumamoto, 860-8555, Japan

Bradley D. Johnson
US Army Engineering Research and Development Center
3909 Halls Ferry Road, Vicksburg, MS 39180-6199, USA

Simple formulas for the cross-shore and longshore transport rates of suspended sand and bedload on beaches are proposed by synthesizing available data and formulas. A combined wave and current model based on the time-averaged continuity, momentum, and energy equations for water is improved and used to provide hydrodynamic input to the proposed sand transport model. The model is compared with spilling and plunging wave tests conducted in a large wave basin using fine sand. The numeric model predicts the measured longshore suspended sand and total transport rates within a factor of about 2. The longshore bedload transport rate is predicted to be small. The predicted cross-shore sand transport rates are relatively small on the quasi-equilibrium beaches in these tests. The computed beach profile change under 10-h wave action is less than about 5 cm. The proposed sediment transport model will need to be verified using additional data but no bedload data is available in surf zones and reliable suspended load data is scarce.

28.1. Introduction

The predictive capability of sediment transport on beaches is essential for coastal sediment management, beach nourishment and storm damage reduction, and dredging of navigation channels. A large number of studies have been conducted to obtain sediment transport data in laboratories and on natural beaches and to develop predictive sediment transport models. However, none of the existing transport models are reliable and robust unlike coastal wave and current models that have been improved steadily for the past 30 years. The major reason for this discrepancy is that no dynamic equation is available to describe the motion of a large number of sediment particles. Consequently, existing sediment transport models are essentially empiric and dependent on reliable sediment data. Unfortunately, sediment dynamics on beaches are highly complex and involve wide ranges of morphologic scales in time and space. Correspondingly, available sediment transport models have become more complex but less robust. In view of the empiric nature of any sediment transport model, it is desirable to develop a simple but robust model that synthesizes the existing formulas for sediment transport on beaches. Furthermore, the sediment transport model should be very efficient computationally because the model will need to be calibrated and verified using extensive data sets.

This chapter presents our recent efforts to develop and calibrate a sand transport model that is suited for practical applications but contains the basic mechanics of sand suspension and bedload movement on beaches. The hydrodynamic input required for the sand transport model is limited to the variables of irregular waves and currents which can be predicted efficiently and fairly accurately using a combined wave and current model based on time-averaged continuity, momentum, and energy equations. More advanced but computationally-demanding wave and current models may not improve the accuracy of the sand transport model with errors of a factor of about 2. Moreover, practical coastal sediment problems require the prediction of sediment transport rates for a duration of days to years. The computational efficiency is hence essential for practical applications.

This chapter is organized as follows. Section 28.2 presents the combined wave and current model which is presently limited to the case of alongshore uniformity and unidirectional irregular waves. Section 28.3 shows new formulas for the cross-shore and longshore transport rates of suspended sand and bedload where the proposed formulas are presently limited to uniform sand. The beach profile evolution is computed using the standard continuity equation of bottom sand. Section 28.4 compares the sediment formulas with the spiling and plunging wave tests conducted in the Large-scale Sediment Transport Facility at the US Army Engineer Research and Development Center. Section 28.5 summarizes the findings of this chapter and discusses future work.

28.2. Combined Wave and Current Model

The combined wave and current model in the following is an extension of the time-averaged model developed by Kobayashi *et al.*[1] on the basis of the Dutch

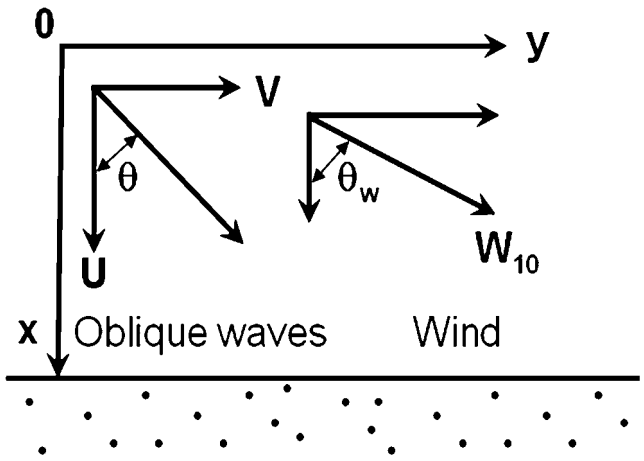

Fig. 28.1. Incident irregular waves and wind on beach of alongshore uniformity.

models by Reniers and Battjes[2] and Ruessink *et al.*[3] Figure 28.1 shows obliquely incident irregular waves on a straight shoreline where the cross-shore coordinate x is positive onshore, and the longshore coordinate y is positive in the downwave direction. The depth-averaged cross-shore and longshore velocities are denoted by U and V, respectively. Incident waves are assumed to be unidirectional with θ is the incident angle relative to the shore normal and uniform in the longshore direction. The wave angle θ is assumed to be in the range of $|\theta| < 90^\circ$ to ensure that the incident waves propagate landward. The wind speed and direction at the elevation of 10 m above the sea surface are denoted by W_{10} and θ_w, respectively.

The governing equations for water under the assumption of alongshore uniformity are averaged over a number of wind waves to obtain the time-averaged equations. The beach is assumed to be impermeable where Kobayashi *et al.*[4] included a permeable layer for the case of normally incident waves. The depth-integrated continuity equation of water requires that the cross-shore volume flux is zero in the absence of wave overtopping where Kobayashi *et al.*[5] analyzed irregular wave overtopping of permeable slopes. The requirement of zero cross-shore volume flux is expressed as

$$\bar{h}\,\bar{U} + \frac{g\sigma_\eta^2}{C_p}\cos\theta + q_r\cos\theta = 0 \tag{28.1}$$

where $\bar{h}$ is the mean water depth given by $\bar{h} = (\bar{\eta} - z_b)$, with $\bar{\eta}$ the mean free surface elevation and z_b the bottom elevation; $\bar{U}$ is the mean cross-shore velocity, which is negative and offshore because $\cos\theta > 0$; g is the gravitational acceleration; σ_η, the standard deviation of the free surface elevation η; C_p, the linear wave phase velocity in the mean water depth $\bar{h}$ corresponding to the spectral peak period T_p; and q_r, the volume flux of a roller on the front of a breaking wave. The second term on the left-hand side of Eq. (28.1) is the onshore volume flux due to linear waves

propagating in the direction of θ (e.g., Ref. 6) where the representative period of irregular waves is chosen as the peak period T_p specified at the seaward boundary $x = 0$. Snell's law is used to obtain the wave direction θ

$$\sin\theta/C_p = \text{constant} \tag{28.2}$$

where the constant value is obtained from the values of θ, $\bar{h}$, and T_p specified at $x = 0$. Reflected waves are neglected in this model.

The cross-shore and longshore momentum equations are expressed as

$$\frac{dS_{xx}}{dx} = -\rho g\bar{h}\frac{d\bar{\eta}}{dx} - \tau_{bx} + \tau_{wx} \tag{28.3}$$

$$\frac{dS_{xy}}{dx} = -\tau_{by} + \tau_{wy} \tag{28.4}$$

where S_{xx} is the cross-shore radiation stress; ρ, water density; τ_{bx}, cross-shore bottom stress; τ_{wx}, cross-shore wind stress on the sea surface; S_{xy}, shear component of the radiation stress; τ_{by}, longshore bottom stress; and τ_{wy}, longshore wind stress on the sea surface. The wind shear stresses may not be negligible especially outside surf zones on natural beaches.[7] Linear wave theory for progressive waves are used to estimate S_{xx} and S_{xy}

$$S_{xx} = (nE + M_r)\cos^2\theta + E\left(n - \frac{1}{2}\right); \quad S_{xy} = (nE + M_r)\cos\theta\sin\theta \tag{28.5}$$

with

$$n = C_g/C_p; \quad E = \rho g\sigma_\eta^2; \quad M_r = \rho C_p q_r \tag{28.6}$$

where C_g is the linear wave group velocity based on $\bar{h}$ and T_p; E, specific wave energy with the root-mean-square wave height defined as $H_{\text{rms}} = \sqrt{8}\sigma_\eta$; and M_r, momentum flux of a roller propagating with the phase velocity C_p.

The time-averaged bottom shear stresses are written as

$$\tau_{bx} = \frac{1}{2}\rho f_b\overline{UU_a}; \quad \tau_{by} = \frac{1}{2}\rho f_b\overline{VU_a}; \quad U_a = (U^2 + V^2)^{0.5} \tag{28.7}$$

where f_b is the bottom friction factor, and the overbar indicates time averaging. The bottom friction factor f_b is of the order of 0.015 and should be calibrated using longshore current data because of the sensitivity of longshore currents to f_b. The equivalency of the time and probabilistic averaging is assumed to express τ_{bx} and τ_{by} in terms of the mean and standard deviation of the depth-averaged velocities U and V expressed as

$$U = \sigma_T F_U; \quad V = \sigma_T F_V; \quad U_a = \sigma_T F_a; \quad F_a = (F_U^2 + F_V^2)^{0.5} \tag{28.8}$$

with

$$F_U = U_* + r\cos\theta; \quad F_V = V_* + r\sin\theta; \quad U_* = \frac{\bar{U}}{\sigma_T}; \quad V_* = \frac{\bar{V}}{\sigma_T} \tag{28.9}$$

where $\bar{U}$ and $\bar{V}$ are the depth-averaged cross-shore and longshore currents; σ_T, the standard deviation of the oscillatory (assumed Gaussian) depth-averaged velocity U_T with zero mean; and r, the Gaussian variable defined as $r = U_T/\sigma_T$ whose probability density function is given by

$$f(r) = \frac{1}{\sqrt{2\pi}} \exp\left(-\frac{r^2}{2}\right). \tag{28.10}$$

Linear progressive wave theory is used locally to express U_T in terms of the oscillatory free surface elevation $(\eta - \bar{\eta})$

$$U_T = \frac{C_p}{\bar{h}}(\eta - \bar{\eta}) \tag{28.11}$$

which yields the standard deviation σ_T of the oscillatory velocity U_T

$$\sigma_T = C_p \sigma_*; \quad \sigma_* = \sigma_\eta/\bar{h}. \tag{28.12}$$

It is noted that $U_* = \bar{U}/\sigma_T$ and $V_* = \bar{V}/\sigma_T$ are of the order of unity or less. The standard deviations of U and V are given by

$$\sigma_U = \sigma_T \cos\theta; \quad \sigma_V = \sigma_T |\sin\theta| \tag{28.13}$$

where $\cos\theta > 0$ but $\sin\theta$ can be negative. Substitution of Eq. (28.8) into Eq. (28.7) yields

$$\tau_{bx} = \frac{1}{2}\rho f_b \sigma_T^2 G_{bx}; \quad \tau_{by} = \frac{1}{2}\rho f_b \sigma_T^2 G_{by} \tag{28.14}$$

with

$$G_{bx} = \int_{-\infty}^{\infty} F_U F_a f(r) dr; \quad G_{by} = \int_{-\infty}^{\infty} F_V F_a f(r) dr \tag{28.15}$$

which must be integrated numerically.

The wind shear stresses are expressed as

$$\tau_{sx} = \rho_a C_D W_{10}^2 \cos\theta_w; \quad \tau_{sy} = \rho_a C_D W_{10}^2 \sin\theta_w \tag{28.16}$$

where ρ_a is the air density ($\rho_a \simeq 1.225\,\mathrm{kg/m^3}$); C_D, the drag coefficient, W_{10}, the 10-m wind speed; and θ_w, the wind direction defined in Fig. 28.1. The formula by Large and Pond[8] is used to estimate C_D where $C_D = 0.0012$ for $W_{10} < 11\,\mathrm{m/s}$ and $C_D = (0.00049 + 0.000065\,W_{10})$ for $W_{10} \geq 11\,\mathrm{m/s}$. It is noted that the measured values of C_D during tropical cyclones by Powell *et al.*[9] indicated no increase of C_D with the increase of W_{10} much above 25 m/s. In short, available data is insufficient to estimate C_D for extreme wind conditions.

The wave energy equation is written as

$$\frac{dF_x}{dx} = -D_B - D_f; \quad F_x = EC_g \cos\theta \tag{28.17}$$

where F_x is the cross-shore energy flux based on linear progressive wave theory, and D_B and D_f are the energy dissipation rates due to wave breaking and bottom friction, respectively. The energy dissipation rate D_B due to wave breaking in Eq. (28.17) is estimated using the formula by Battjes and Stive,[10] which was modified by Kobayashi *et al.*[11] to account for the local bottom slope and to extend the computation to the lower swash zone. The breaker ratio parameter γ in this formula is typically in the range of $\gamma = 0.5$–1.0,[1] but should be calibrated to obtain a good agreement with the measured cross-shore variation of σ_η if such data is available. The energy dissipation rate D_f due to bottom friction is expressed as

$$D_f = \frac{1}{2}\rho f_b \overline{U_a^3}. \tag{28.18}$$

Substitution of U_a given in Eq. (28.8) into Eq. (28.18) yields

$$D_f = \frac{1}{2}\rho f_b \sigma_T^3 G_f; \quad G_f = \int_{-\infty}^{\infty} F_a^3 f(r) dr \tag{28.19}$$

where F_a and $f(r)$ are given in Eqs. (28.8)–(28.10).

The energy equation for the roller represented by its volume flux q_r may be expressed as[3]

$$\frac{\mathrm{d}}{\mathrm{d}x}\left(\rho C_p^2 q_r \cos\theta\right) = D_B - D_r; \quad D_r = \rho g \beta_r q_r \tag{28.20}$$

where the roller dissipation rate D_r is assumed to equal the rate of work to maintain the roller on the wave-front slope β_r of the order of 0.1. Use is made of the empiric formula for β_r proposed by Kobayashi *et al.*[11] who included the local bottom slope effect. If the roller is neglected, $q_r = 0$ and Eq. (28.20) yields $D_r = D_B$. The roller effect is included in the subsequent computation to improve the agreement for the longshore current.[1]

Equations (28.1)–(28.20) are the same as those used by Kobayashi *et al.*[17] who neglected the wind shear stresses in Eqs. (28.3) and (28.4) and used linear shallow-water wave theory with $C_p = (g\bar{h})^{0.5}$ in Eq. (28.11). Substitution of Eqs. (28.12) and (28.13) into Eq. (28.1) yields

$$\bar{U} = -\frac{g\bar{h}}{C_p^2}\sigma_U \sigma_* \left(1 + \frac{C_p q_r}{g\sigma_\eta^2}\right) \tag{28.21}$$

which reduces to the equation used by Kobayashi *et al.*[1] in shallow water. The landward-marching computation starting from $x = 0$ outside the surf zone is the same as before. Approximate analytic equations of G_{bx}, G_{by}, and G_f given by Eqs. (28.15) and (28.19) are obtained in the following to reduce the computation time and improve the numeric stability.

The function F_a given in Eq. (28.8) with Eq. (28.9) is rewritten as

$$F_a = \left[(r - r_m)^2 + F_m^2\right]^{0.5} \tag{28.22}$$

with

$$r_m = -(U_* \cos\theta + V_* \sin\theta); \quad F_m = V_* \cos\theta - U_* \sin\theta. \tag{28.23}$$

Equation (28.22) is approximated as

$$\begin{aligned} F_a &= (r - r_m) + |F_m| \quad \text{for } r \geq 0 \\ F_a &= -(r - r_m) + |F_m| \quad \text{for } r < 0. \end{aligned} \tag{28.24}$$

Substituting Eq. (28.24) into Eqs. (28.15) and (28.19) and integrating the resulting equations analytically, we obtain approximate expressions for G_{bx}, G_{by}, and G_f

$$G_{bx} = \sqrt{\frac{2}{\pi}}(U_* - r_m \cos\theta) + U_*|F_m| \tag{28.25}$$

$$G_{by} = \sqrt{\frac{2}{\pi}}(V_* - r_m \sin\theta) + V_*|F_m| \tag{28.26}$$

$$G_f = 2\sqrt{\frac{2}{\pi}} + (1 + U_*^2 + V_*^2)|F_m| + \sqrt{\frac{2}{\pi}}\left(U_*^2 + V_*^2 + 2r_m^2\right) \tag{28.27}$$

which depends on $\sin\theta$ ($\cos\theta > 0$ assumed), r_m and F_m where Eq. (28.23) yields $U_* = -(r_m \cos\theta + F_m \sin\theta)$ and $V_* = (F_m \cos\theta - r_m \sin\theta)$.

For the case of normally incident waves with no wind, $\sin\theta = 0$ and $V_* = 0$. Equations (28.25)–(28.27) yield $G_{bx} = 1.6\ U_*$, $G_{by} = 0$, and $G_f = (1.6 + 2.4\ U_*^2)$. For this case, Eq. (28.4) requires $\tau_{by} = 0$ and Eq. (28.14) yields $G_{by} = 0$. As a result, Eq. (28.26) is exact. For $\sin\theta = 0$ and $V_* = 0$, G_{bx} and G_f given by Eqs. (28.15) and (28.19) can be integrated analytically as presented by Kobayashi *et al.*[4] who approximated the analytic expressions of G_{bx} and G_f as $G_{bx} = 1.64\ U_*$ and $G_f = (1.6 + 2.6\ U_*^2)$. These approximate equations are very similar to the above equations obtained from Eqs. (28.25) and (28.27).

For the case of $|\sin\theta| \ll 1$ and $|U_*| \ll |V_*|$, Eq. (28.26) can be approximated as $G_{by} = V_*(0.8 + |V_*|)$. Using field data and probabilistic analyses, Feddersen *et al.*[12] obtained $G_{by} = V_*(1.16^2 + V_*^2)^{0.5}$. The difference between these two approximate equations for G_{by} is less than 20% for $|V_*| < 1.4$, which is typically satisfied.

Finally, the approximate values of G_{bx}, G_{by}, and G_f given by Eqs. (28.25)–(28.27) are compared with the exact values of G_{bx}, G_{by}, and G_f obtained by the numeric integration of Eqs. (28.15) and (28.19). The percentage error E_p is defined as

$$E_p = \frac{100 \times |\text{exact value} - \text{approximate value}|}{|\text{exact value}|}.$$

The values of E_P for G_{bx}, G_{by}, and G_f are computed for the ranges of $|\sin\theta| < 1$, $|r_m| < 1$, and $|F_m| < 1$. The maximum value of E_p with respect to $\sin\theta$ for given r_m and F_m is obtained and plotted in Fig. 28.2. The percentage error increases with the increase of $|r_m|$ and $|F_m|$ because of the approximation of F_a given by Eq. (28.24), which is exact only when $r_m = 0$ and $F_m = 0$. The maximum error in Fig. 28.2 is less than 35%. This error is probably less than the uncertainty of the bottom friction factor f_b involved in τ_{bx}, τ_{by}, and D_f in Eqs. (28.14) and (28.19). Consequently, Eqs. (28.25)–(28.27) are adopted here for computational efficiency and stability. It is noted that the longshore momentum equation (28.4) is solved numerically to obtain τ_{by} and G_{by} by use of Eq. (28.14). Equation (28.26) is solved

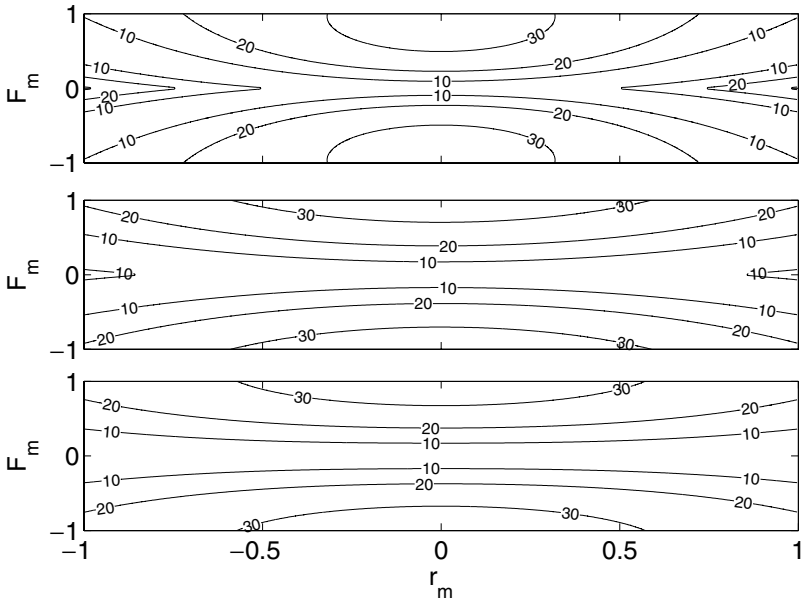

Fig. 28.2. Contours of maximum percentage error with respect to $\sin\theta$ as a function of r_m and F_m for G_{bx} (top), G_{by} (middle), and G_f (bottom).

analytically to obtain the longshore current $\bar{V}$ for the computed G_{by}. This implicit numeric procedure improves the numeric stability of the computation marching in x (similar to time).

28.3. Sediment Transport Model

The combined wave and current model predicts the cross-shore variations of the hydrodynamic variables used in the following sediment transport model for given beach profile, water level, and seaward wave conditions at $x = 0$. The bottom sediment is assumed to be uniform and characterized by d_{50}, the median diameter; w_f, sediment fall velocity; and s, sediment specific gravity.

First, the cross-shore variation of the degree of sediment movement is estimated using the critical Shields parameter ψ_c[13] which is taken as $\psi_c = 0.05$. The instantaneous bottom shear stress τ_b' is assumed to be given by $\tau_b' = 0.5\ \rho f_b U_a^2$ with U_a given in Eq. (28.8). The sediment movement is assumed to occur when $|\tau_b'|$ exceeds the critical shear stress, $\rho g(s-1)d_{50}\psi_c$. The probability P_b of sediment movement can be shown to be the same as the probability of $(r - r_m)^2 > F_b^2 = (R_b^2 - F_m^2)$ where $R_b = [2g(s-1)d_{50}\psi_c f_b^{-1}]^{0.5}/\sigma_T$ and r_m and F_m are defined in Eq. (28.23). For the Gaussian variable r given by Eq. (28.10), P_b is given by

$$P_b = \frac{1}{2}\mathrm{erf}\, c\left(\frac{F_b - r_m}{\sqrt{2}}\right) + \frac{1}{2}\mathrm{erf}\, c\left(\frac{F_b + r_m}{\sqrt{2}}\right) \quad \text{for } F_b^2 > 0 \tag{28.28}$$

and $P_b = 1$ for $F_b^2 \leq 0$ where $\mathrm{erf}\, c$ is the complementary error function. The value of P_b computed from $x = 0$ located outside the surf zone increases landward and fluctuates in the surf and swash zones, depending on the presence of a bar or a terrace that increases the local fluid velocity.

Second, the cross-shore variation of the degree of sediment suspension is estimated using the experimental finding of Kobayashi *et al.*[11] who showed that the turbulent velocities measured in the vicinity of the bottom were related to the energy dissipation rate due to bottom friction. Representing the magnitude of the instantaneous turbulent velocity by $(D'_f/\rho)^{1/3}$ with $D'_f = 0.5\rho f_b U_a^3$ in light of Eq. (28.18), the probability P_s of sediment suspension is assumed to be the same as the probability of $(D'_f/\rho)^{1/3}$ exceeding the sediment fall velocity w_f. The probability P_s is then equal to the probability of $(r - r_m)^2 > F_s^2 = (R_s^2 - F_m^2)$ with $R_s = [(2/f_b)^{1/3} w_f/\sigma_T]$ and is given by

$$P_s = \frac{1}{2}\mathrm{erf}\, c\left(\frac{F_s - r_m}{\sqrt{2}}\right) + \frac{1}{2}\mathrm{erf}\, c\left(\frac{F_s + r_m}{\sqrt{2}}\right) \quad \text{for } F_s^2 > 0 \tag{28.29}$$

and $P_s = 1$ for $F_s^2 \leq 0$. If $P_s > P_b$, use is made of $P_s = P_b$ assuming that sediment suspension occurs only when sediment movement occurs. Fine sands on beaches tend to be suspended once their movement is initiated.

Third, the suspended sediment volume V_s per unit horizontal bottom area is estimated by modifying the sediment suspension model by Kobayashi and Johnson[14]

$$V_s = P_s \frac{e_B D_r + e_f D_f}{\rho g(s-1) w_f}(1 + S_b^2)^{0.5}; \quad S_b = \frac{dz_b}{dx} \tag{28.30}$$

where S_b is the cross-shore bottom slope; and e_B and e_f are the suspension efficiencies for the energy dissipation rates D_r and D_f due to wave-breaking and bottom friction in Eqs. (28.17) and (28.20), respectively. Use is made of $e_B = 0.002$ and $e_f = 0.01$ adopted by Kobayashi *et al.*[1] but the value of e_B is uncertain and should be calibrated if V_s is measured.[15] The sediment suspension probability P_s is added in Eq. (28.30) to ensure $V_s = 0$ if $P_s = 0$. The term $(1 + S_b^2)^{0.5}$ is the actual bottom area per unit horizontal bottom area and essentially unity except for very steep slopes. The cross-shore and longshore suspended sediment transport rates q_{sx} and q_{sy} are expressed as

$$q_{sx} = a\bar{U}V_s; \quad q_{sy} = \bar{V}V_s \tag{28.31}$$

where a is the empiric suspended load parameter. The parameter a accounts for the onshore suspended sediment transport due to the positive correlation between the time-varying cross-shore velocity and suspended sediment concentration. The value of a increases to unity as the positive correlation decreases to zero. For the three small-scale equilibrium profile tests conducted by Kobayashi *et al.*,[11] a was of the order of 0.2. Use is made of $a = 0.2$ in the subsequent computation. The cross-shore suspended sediment transport rate q_{sx} is negative (offshore) because the return (undertow) current $\bar{U}$ is negative (offshore). On the other hand, the longshore suspended sediment transport rate q_{sy} in Eq. (28.31) neglects the correlation between the time-varying longshore velocity and suspended sediment concentration, which appears to be very small if the longshore current $\bar{V}$ is sufficiently large.

Fourth, the formulas for the cross-shore and longshore bedload transport rates q_{bx} and q_{by} are devised somewhat intuitively because bedload in the surf zone has never been measured. The time-averaged rates q_{bx} and q_{by} are tentatively expressed as

$$q_{bx} = B\overline{(U^2+V^2)U}; \quad q_{by} = B\overline{(U^2+V^2)V} \tag{28.32}$$

where B is the empiric parameter. Equation (28.32) may be regarded as a quasi-steady application of the formula of Meyer-Peter and Mueller (e.g., Ref. 16). Substitution of U and V given in Eq. (28.8) with Eqs. (28.9) and (28.10) into Eq. (28.32) yields

$$q_{bx} = B\sigma_T^3(b_* + U_*V_*^2 + 2F_m \sin\theta) \tag{28.33}$$

$$q_{by} = B\sigma_T^3[V_*(1+U_*^2+V_*^2) - 2r_m \sin\theta] \tag{28.34}$$

where $b_* = (3U_* + U_*^3)$, and F_m and r_m are defined in Eq. (28.23).

Equations (28.33) and (28.34) yield $q_{bx} = b_*B\sigma_T^3$ and $q_{by} = 0$ for normally incident waves with $\sin\theta = 0$ and $V_* = 0$. The expressions of B and b_* are obtained by requiring that $q_{bx} = b_*B\sigma_T^3$ reduces to the onshore bedload formula proposed by Kobayashi *et al.*[17] for normally incident waves. This formula was shown to synthesize existing data and simple formulas. The proposed formulas are written as

$$q_{bx} = \frac{bP_b}{g(s-1)}\sigma_T^3(1 + U_*V_*^2 + 2F_m \sin\theta)G_s \tag{28.35}$$

$$q_{by} = \frac{bP_b}{g(s-1)}\,\sigma_T^3[V_*(1+U_*^2+V_*^2) - 2r_m \sin\theta] \tag{28.36}$$

where b is the empiric bedload parameter, and G_s, the bottom slope function. The sediment movement probability P_b given in Eq. (28.28) accounts for the initiation of sediment movement. It is noted that $b_* = 1$ in Eq. (28.35) to compensate for the limitations of Eq. (28.32) and the Gaussian distribution of the horizontal velocity used in Eqs. (28.9) and (28.10) as discussed by Kobayashi *et al.*[17] They calibrated $b = 0.002$ using the 20 water tunnel tests of Ribberink and Al-Salem[18] and the four large-scale wave flume tests of Dohmen-Janssen and Hanes.[19] However, these tests were conducted for nonbreaking waves and the assumed value of $b = 0.002$ is uncertain in surf and swash zones.

The bottom slope function G_s was introduced by Kobayashi *et al.*[17] to account for the effect of the steep cross-shore slope S_b on the bedload transport rate and is expressed as

$$G_s = \tan\phi/(\tan\phi + S_b) \quad \text{for } -\tan\phi < S_b < 0 \tag{28.37}$$

$$G_s = (\tan\phi - 2S_b)/(\tan\phi - S_b) \quad \text{for } 0 < S_b < \tan\phi \tag{28.38}$$

where ϕ is the angle of internal friction of the sediment and $\tan\phi \simeq 0.63$ for sand.[20] For $S_b = 0$, $G_s = 1$. Equation (28.37) corresponds to the functional form of G_s

used by Bagnold[21] for steady stream flow on a downward slope with $S_b < 0$ where the downward slope increases q_{bx}. Equation (28.38) ensures that G_s approaches negative infinity as the upward slope S_b approaches $\tan\phi$ and that Eqs. (28.37) and (28.38) reduce to $G_s \simeq (1 - S_b/\tan\phi)$ for $|S_b| \ll \tan\phi$. Equation (28.35) with G_s given by Eqs. (28.37) and (28.38) implies that the bedload transport rate q_{bx} is positive (onshore) for $S_b < (\tan\phi)/2$ and negative (offshore) for $S_b > (\tan\phi)/2$. Use is made of $|G_s| < G_m = 10$ to avoid an infinite value in the computation. The computed profile change is not very sensitive to the assumed value of G_m because the beach profile changes in such a way to reduce a very steep slope except in the region of scarping.

The landward marching computation of the present time-averaged model ends at the cross-shore location $x = x_m$ where the mean water depth $\bar{h}$ is less than 1 cm. The probabilistic model by Kobayashi *et al.*[22] could be used to predict the irregular wave runup distribution but no reliable data exists for suspended sand and bedload transport rates in the zone which is wet and dry intermittently. Consequently, the following simple procedure is adopted to deal with the zone with the bottom slope $S_b > \tan\phi$. The cross-shore total sediment transport rate $q_x = (q_{sx} + q_{bx})$ at $x = x_m$ is denoted by q_{xm}. If q_{xm} is negative (offshore), q_x is extrapolated linearly to estimate q_x on the scarped face with $S_b > \tan\phi$

$$q_x = q_{xm}(x_e - x)/(x_e - x_m) \quad \text{for } x_m < x < x_e \tag{28.39}$$

where x_e is the landward limit of the scarping zone with $S_b > \tan\phi$. The extrapolated q_x is in the range of $q_{xm} \le q_x \le 0$ and the scarping zone is eroded due to the offshore sediment transport. This simple procedure does not allow onshore sediment transport due to overwash.

Finally, the cross-shore beach profile change is computed using the continuity equation of bottom sediment for the case of alongshore uniformity

$$(1 - n_p)\frac{\partial z_b}{\partial t} + \frac{\partial q_x}{\partial x} = 0 \tag{28.40}$$

where n_p is the porosity of the bottom sediment which is assumed to be $n_p = 0.4$, and t, slow morphologic time for the change of the bottom elevation z_b. Equation (28.40) is solved using an explicit Lax-Wendroff numeric scheme (e.g., Ref. 23) to obtain the bottom elevation at the next time level. This computation procedure is repeated starting from the initial bottom profile until the end of a profile evolution test. The computation time is of the order of 10^{-3} of the test duration.

28.4. Comparison with Data

The present numeric model is compared with the spilling and plunging wave tests conducted in the large-scale sediment transport facility at the US Army Engineer Research and Development Center.[24] Pumps were used to circulate the wave-induced longshore current and establish the alongshore uniformity of hydrodynamics and morphology on the middle section of the quasi-equilibrium beach

Table 28.1. Wave conditions at $x = 0$ for spilling and plunging wave tests.

Breaker	d (cm)	$H_{\rm rms}$ (cm)	θ (deg)	T_p (s)	f_b	γ
Spilling	76.8	18.2	10	1.5	0.02	1.0
Plunging	77.3	18.9	10	3.0	0.02	0.7

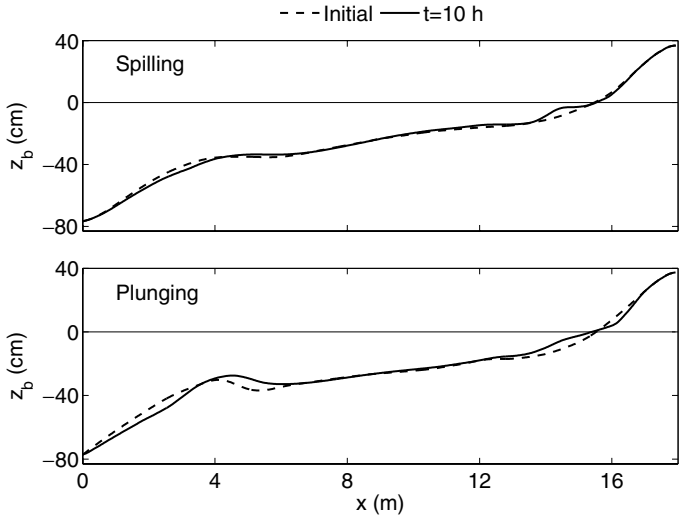

Fig. 28.3. Quasi-equilibrium beach profile (solid line) and computed profile after 10-h wave action (dash line) for spilling and plunging wave tests.

comprised of uniform fine sand with $d_{50} = 0.15\,\text{mm}$, $s = 2.65$, and $w_f = 1.65\,\text{cm/s}$. Table 28.1 lists the wave conditions at the seaward boundary $x = 0$ and the values of the bottom friction factor f_b in Eq. (28.7) and the breaker ratio parameter γ for D_B in Eq. (28.17). These values of f_b and γ are the same as those used in the previous comparison by Kobayashi *et al.*[1] The still water depth d, the root-mean-square wave height $H_{\rm rms} = \sqrt{8}\sigma_\eta$ and the incident unidirectional wave angle θ at $x = 0$ were practically the same for both tests. The major difference was the spectral peak period T_p of the incident waves and the resulting breaker patterns. The quasi-equilibrium beach profiles of the two tests are shown in Fig. 28.3.

Comparisons are made of the measured and computed cross-shore variations of the mean and standard deviation of the free surface elevation η, cross-shore velocity U, and longshore velocity V as well as the suspended sediment volume V_s per unit horizontal bottom area. V_s is predicted using Eq. (28.30) with the sediment suspension probability P_s and the bottom slope effect, which were not included previously. These comparisons are assessed in light of those presented by Agarwal *et al.*[25] and Kobayashi *et al.*[1] The degree of agreement is found to be practically the same. The modifications presented in this chapter change the computed results very little. However, the present computation is more efficient and stable because of the

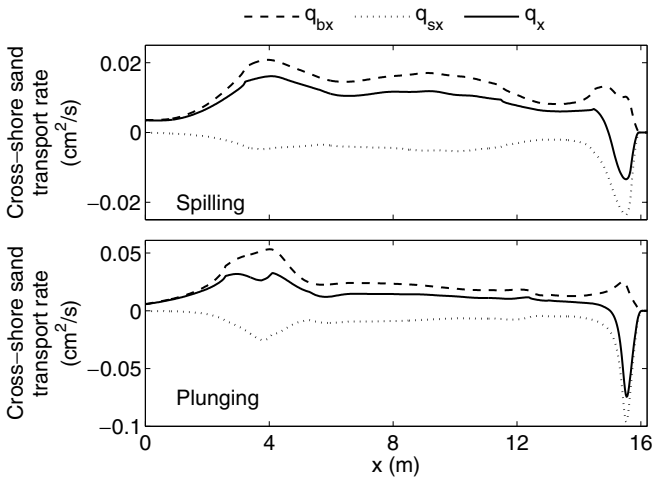

Fig. 28.4. Computed cross-shore sand transport rates q_{bx}, q_{sx}, and $q_x = (q_{bx} + q_{sx})$ for spilling and plunging wave tests.

use of the analytic expressions of G_{bx}, G_{by}, and G_f given by Eqs. (28.25)–(28.27). The roller effect represented by the roller volume flux q_r improves the agreement for the longshore current $\bar{V}$ as shown in the previous comparisons. The computed sediment transport rates with the roller effect are presented in the following.

Figure 28.4 shows the computed cross-shore variations of q_{bx}, q_{sx}, and q_x for the spilling and plunging wave tests. The cross-shore bedload transport rate q_{bx} is positive (onshore), whereas the cross-shore suspended sand transport rate q_{sx} is negative (offshore). The absolute values of q_{bx} and q_{sx} are larger in the breaker zone near $x = 4\,\mathrm{m}$ and near the still water shoreline, especially for the plunging waves. The computed total sand transport rate $q_x = (q_{bx} + q_{sx})$ is positive (onshore) except in the zone near the shoreline where $q_x < 0$. The absolute value of q_x is less than about $0.05\,\mathrm{cm}^2/\mathrm{s}$ but $q_x = 0$ is required on the equilibrium beach. Consequently, the profile evolution is computed using the measured quasi-equilibrium profile as the initial profile. The initial profile is exposed to the wave conditions listed in Table 28.1 for 10 hours. The computed profile is shown in Fig. 28.3. The computed change of the bottom elevation z_b is less than about 5 cm. The subtle profile change is difficult to predict and measure accurately. It is noted that the fluid velocity and suspended sand concentration were not measured synchronously in these tests, resulting in no measurement of q_{sx}.

Figure 28.5 shows the computed cross-shore variations of q_{by}, q_{sy}, and $q_y = (q_{by} + q_{sy})$. The longshore bedload transport rate q_{by} is positive (downwave) and small in comparison with the longshore suspended sand transport rate q_{sy}. The longshore total sand transport rate q_y is dominated by q_{sy} in these tests using the fine sand with $d_{50} = 0.15\,\mathrm{mm}$ and $w_f = 1.65\,\mathrm{cm/s}$. The longshore sand transport rate q_y is larger under the plunging waves by a factor of more than 2. The comparison of Figs. 28.4 and 28.5 indicates that the longshore sand transport q_y exceeds the cross-shore transport rate q_x by a factor of about 5.

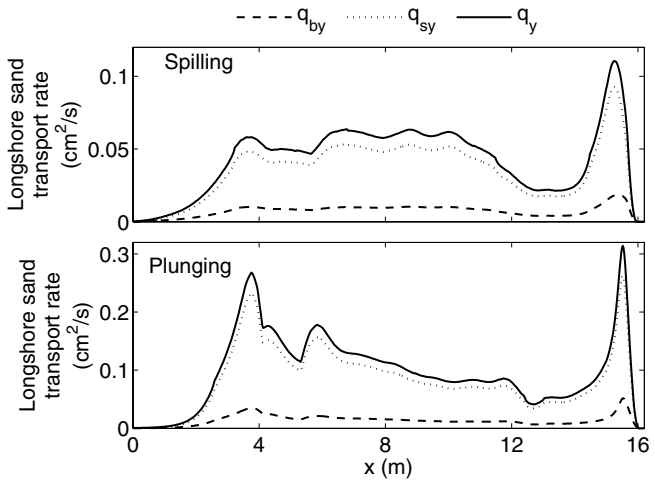

Fig. 28.5. Computed longshore sand transport rates q_{by}, q_{sy}, and $q_y = (q_{by} + q_{sy})$ for spilling and plunging wave tests.

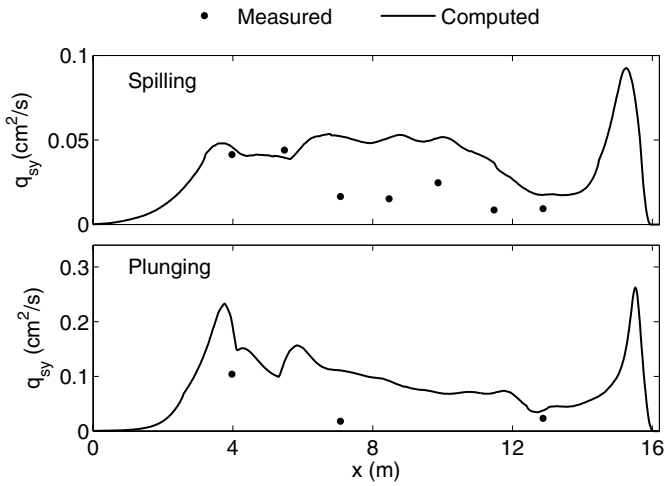

Fig. 28.6. Measured and computed longshore suspended sand transport rates for spilling and plunging wave tests.

Figure 28.6 compares the measured and predicted longshore suspended sand transport rates. The measured q_{sy} was obtained by integrating the product of the measured mean longshore velocity and mean sand concentration vertically as explained by Kobayashi *et al.*[1] The numeric model overpredicts q_y in the middle of the surf zone by a factor of about 2 perhaps because Eq. (28.30) does not account for the downward decay of turbulence generated by broken waves landward of the breaker zone.

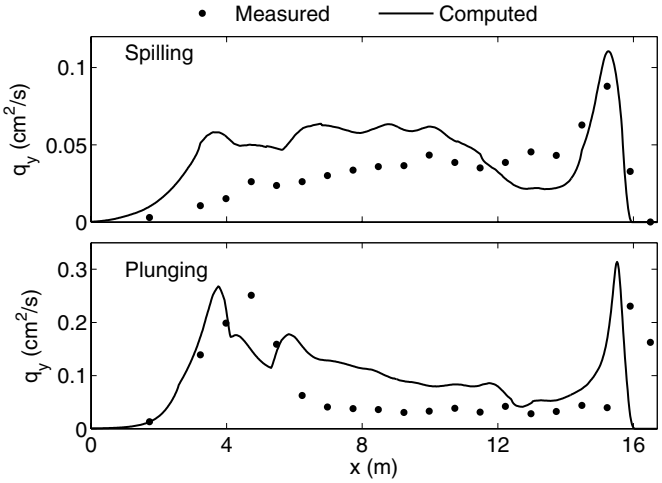

Fig. 28.7. Measured and computed longshore total sand transport rates for spilling and plunging wave tests.

Figure 28.7 compares the measured and predicted longshore total sand transport rates. The measured q_y was obtained from the volume of sand collected in each of 20 downdrift bottom traps. This time-averaged model predicts the large sand transport rate near the shoreline fairly well. The overall agreement is within a factor of about 2. The difference in the cross-shore distributions of q_y under the spilling and plunging waves is predicted by the present time-averaged model.

28.5. Conclusions

The combined wave and current model for obliquely incident waves by Kobayashi *et al.*[1] is improved by including the finite-depth effect on the relationship between the oscillatory horizontal velocity and free surface elevation as well as the wind stresses for future field applications. The numeric integrations involved in the bottom shear stresses and energy dissipation rate are replaced by sufficiently accurate analytic expressions. These modifications improve the computational efficiency and numeric stability of the wave and current model. The sediment transport model developed by Kobayashi *et al.*[11,17] for normally incident waves is extended to include obliquely incident waves and longshore currents. The probabilities of sediment movement and suspension are proposed to account for the initiation of sediment movement and suspension under irregular waves. The cross-shore and longshore suspended sediment transport rates are expressed in terms of the suspended sediment volume per unit horizontal area and the cross-shore and longshore currents. The onshore transport due to the correlation between the cross-shore velocity and suspended sand concentration is taken into account. The cross-shore and longshore bedload transport rates are estimated using a formula similar to that by

Meyer-Peter and Mueller that reduces to the bedload formula by Kobayashi *et al.*[17] for normally incident waves.

The new sediment transport model coupled with the improved wave and current model is compared with spilling and plunging wave tests conducted in a large wave basin using fine sand. The coupled model predicts the measured longshore suspended sand and total transport rates within a factor of about 2. The longshore bedload transport rate is predicted to be small in comparison with the corresponding suspended sand transport rate. The cross-shore sand transport rates were not measured in these quasi-equilibrium beach tests. The coupled model predicts only slight beach profile changes after 10-h wave action in these tests. However, subtle profile changes are difficult to predict and measure accurately.

The coupled numeric model will need to be compared with field data to demonstrate its utility for practical applications. The assumptions of longshore uniformity and uniform sediment are too restrictive on natural beaches. The cross-shore one-dimensional model may be extended to a horizontally two-dimensional model without much difficulty but available sediment transport data is scarce in surf and swash zones. For the prediction of long-term morphologic changes, a method for long-term and spatial averaging will need to be devised to compute morphologic changes for years.

Acknowledgments

This study was supported by the MORPHOS Project of the US Army Corps of Engineers, Coastal and Hydraulics Laboratory. The second author was supported by the Spanish Postdoctoral Scholarship MEC/FULBRIGHT.

References

1. N. Kobayashi, A. Agarwal and B. D. Johnson, Longshore current and sediment transport on beaches, *J. Waterw. Port Coast. Ocean Eng.* **133**(4), 296–304 (2007).
2. A. J. H. M. Reniers and J. A. Battjes, A laboratory study of longshore currents over barred and non-barred beaches, *Coast. Eng.* **30**, 1–21 (1997).
3. B. G. Ruessink, J. R. Miles, F. Feddersen, R. T. Guza and S. Elgar, Modeling the alongshore current on barred beaches, *J. Geophys. Res.* **106**(C10), 22451–22463 (2001).
4. N. Kobayashi, L. E. Meigs, T. Ota and J. A. Melby, Irregular breaking wave transmission over submerged porous breakwaters, *J. Waterw. Port Coast. Ocean Eng.* **133**(2), 104–116 (2007).
5. N. Kobayashi and F. J. de los Santos, Irregular wave seepage and overtopping of permeable slopes, *J. Waterw. Port Coast. Ocean Eng.* **133**(4), 245–254 (2007).
6. R. G. Dean and R. A. Dalrymple, *Water Wave Mechanics for Engineers and Scientists* (World Scientific, Singapore, 1984).
7. S. Lentz, R. T. Guza, S. Elgar, F. Feddersen and T. H. C. Herbers, Momentum balances on the North Carolina inner shelf, *J. Geophys. Res.* **104**(C8), 18205–18226 (1999).

8. W. G. Large and S. Pond, Open ocean momentum flux measurements in moderate to strong winds, *J. Phys. Oceanogr.* **11**, 324–336 (1981).
9. M. D. Powell, P. J. Vickery and T. A. Reinhold, Reduced drag coefficient for high wind speeds in tropical cyclones, *Nature* **422**, 279–283 (2003).
10. J. A. Battjes and M. J. F. Stive, Calibration and verification of a dissipation model for random breaking waves, *J. Geophys. Res.* **90**(C5), 9159–9167 (1985).
11. N. Kobayashi, H. Zhao and Y. Tega, Suspended sand transport in surf zones, *J. Geophys. Res.* **110**(C12009) (2005), doi: 10.1029/2004JC002853.
12. F. Feddersen, R. T. Guza, S. Elgar and T. H. C. Herbers, Velocity moments in alongshore bottom stress parameterization, *J. Geophys. Res.* **105**(C4), 8673–8686 (2000).
13. O. S. Madsen and W. D. Grant, Quantitative description of sediment transport by waves, *Coast. Eng. 1976, Proc. 15th Coast. Eng. Conf.*, American Society of Civil Engineering, Reston, VA (1976).
14. N. Kobayashi and B. D. Johnson, Sand suspension, storage, advection and settling in surf and swash zones, *J. Geophys. Res.* **106**(C5), 9363–9376 (2001).
15. N. Kobayashi and Y. Tega, Sand suspension and transport on equilibrium beach, *J. Waterw. Port Coast. Ocean Eng.* **128**(6), 234–248 (2002).
16. J. S. Ribberink, Bed-load transport for steady flows and unsteady oscillatory flows, *Coast. Eng.* **34**, 59–82 (1998).
17. N. Kobayashi, A. Payo and L. D. Schmied, Cross-shore suspended sand and bedload transport on beaches, *J. Geophys. Res.* **113**(C07001) (2008), doi: 10.1029/2007JC004203.
18. J. S. Ribberink and A. A. Al-Salem, Sediment transport in oscillatory boundary layers in cases of rippled beds and sheet flow, *J. Geophys. Res.* **99**(C6), 12707–12727 (1994).
19. C. M. Dohmen-Janssen and D. H. Hanes, Sheet flow dynamics under monochromatic nonbreaking waves, *J. Geophys. Res.* **107**(C10), 3149 (2002), doi: 10.1029/2001JC001045.
20. J. A. Bailard, An energetics total load sediment transport model for a plane sloping beach, *J. Geophys. Res.* **86**(C11), 10938–10954 (1981).
21. R. A. Bagnold, An approach to the sediment transport problem from general physics, *U.S. Geol. Surv., Prof. Paper* 422-I (1966).
22. N. Kobayashi, F. J. de los Santos and P. G. Kearney, Time-averaged probabilistic model for irregular wave runup on permeable slopes, *J. Waterw. Port Coast. Ocean Eng.* **134**(2), 88–96 (2008).
23. R. B. Nairn and H. N. Southgate, Deterministic profile modelling of nearshore processes. Part 2. Sediment transport and beach profile development, *Coast. Eng.* **19**, 57–96 (1993).
24. P. Wang, B. A. Ebersole, E. R. Smith and B. D. Johnson, Temporal and spatial variations of surf-zone currents and suspended sediment concentration, *Coast. Eng.* **46**, 175–211 (2002).
25. A. Agarwal, N. Kobayashi and B. D. Johnson, Longshore suspended sediment transport in surf and swash zones, *Coast. Eng. 2006, Proc. 30th Coast. Eng. Conf.*, World Scientific, Singapore (2006).